

Front propagation and pattern formation in anisotropic bistable media

Markus Bär,^{1,2,*} Aric Hagberg,^{3,†} Ehud Meron,^{2,‡} and Uwe Thiele,^{1,4,§}

¹Max-Planck-Institut für Physik komplexer Systeme, Nöthnitzer Strasse 38, 01187 Dresden, Germany

²The Blaustein Institute for Desert Research and the Physics Department, Ben-Gurion University, Sede Boker Campus 84990, Israel

³Center for Nonlinear Studies and T-7, Theoretical Division, Los Alamos National Laboratory, Los Alamos, New Mexico 87545

⁴Instituto Pluridisciplinar, Universidad Complutense Madrid, Paseo Juan XXIII 1, E-28040 Madrid, Spain

(Received 13 September 1999)

The effects of diffusion anisotropy on pattern formation in bistable media are studied using a FitzHugh-Nagumo reaction-diffusion model. A relation between the normal velocity of a front and its curvature is derived and used to identify distinct spatiotemporal patterns induced by the diffusion anisotropy. In a wide parameter range anisotropy is found to have an ordering effect: initial patterns evolve into stationary or breathing periodic stripes parallel to one of the principal axes. In a different parameter range, anisotropy is found to induce spatiotemporal chaos confined to one space dimension, a state we term “stratified chaos.”

PACS number(s): 05.45.-a, 82.20.Mj

I. INTRODUCTION

Broken rotational symmetry is a common feature in a variety of physical, chemical, and biological contexts, including liquid crystals [1], catalytic surface reactions [2], and cardiac tissue [3–5]. It is responsible for pattern formation phenomena not encountered in isotropic systems [6] such as ordered arrays of topological defects [7,8], anisotropic phase turbulence [9], reaction-diffusion waves with sharp corners [10–12], and wave fragments traveling along a preferred orientation [13].

Catalytic surface reactions provide good case models for studying the effects of broken rotational symmetry on pattern formation in reaction-diffusion systems. Experiments can be carried out at steady-state conditions, allowing the study of asymptotic dynamics, and the systems are genuinely two-dimensional, facilitating the comparisons of experiments with simulations and analysis of two-dimensional models. The broken rotational symmetry comes from the inherent anisotropy of the crystal surface structure or from preferred alignment of imperfections on the surface. The amount of anisotropy may change due to surface phase transitions that occur during the reaction [14–17]. The chemical kinetics in catalytic reactions may exhibit excitability of a uniform state or bistability of two uniform states pertaining to different adsorbate coverages. In the latter case fronts separating different uniform states are common spatial structures.

The simplest catalytic system is CO oxidation on Pt(111). Theoretical analysis and recent experiments [18,19] using photoelectron emission microscopy (PEEM) found a unique direction and speed of front propagation. In general, however, the direction of front propagation may not be unique. Coexistence of fronts propagating in opposite directions has been observed in catalytic CO oxidation on platinum sur-

faces that undergo structural changes due to adsorbate-induced phase transitions. Examples include CO oxidation on Pt(110) [20,21], Pt(100) [22], and Pt(210) [23]. Another example is the NO and H₂ reaction on a strongly anisotropic Rh(110) surface [10–12].

The coexistence of counterpropagating fronts has been referred to as “dynamic bistability” (see [24] and references therein) and has been attributed to a front bifurcation that takes a single stable front into a pair of counterpropagating stable fronts [25]. A similar bifurcation has also been found in bulk chemical reactions [26,27] and liquid crystals [28], and is known as a nonequilibrium Ising-Bloch (NIB) bifurcation [29–32]. The NIB bifurcation designates the border line between uniform states or stationary patterns and traveling waves [30,31,33]. The fronts may also be unstable to perturbations in the transverse direction (along the front). The coupling of a transverse instability with the NIB bifurcation in isotropic media may produce complex spatiotemporal phenomena involving spontaneous nucleation of spiral waves followed by domain breakup [34–37].

In this paper we study front dynamics and pattern formation in a two-dimensional bistable reaction-diffusion system with anisotropic diffusion. The system has both a NIB bifurcation and transverse instability of planar fronts. We study the angular dependence of front properties by deriving relations between the normal front velocity and its curvature. These relations are used to extract information about the number, velocity, and stability of planar front solutions. We focus on cases where fronts propagating in different directions have different properties. For example, fronts propagating in the x direction may be unstable to transverse perturbations, while those traveling in the y direction are stable. The information from the velocity-curvature relations is then used to motivate a search in parameter space for new pattern formation mechanisms. Numerical solutions of the reaction-diffusion system are used to identify these new patterns. We do not use the velocity-curvature relations to evolve front lines in time as was done in other contexts [38–40]. In our case the proximity to the NIB bifurcation requires treating the normal front velocity as an independent dynamical variable. We further elaborate on this point in Sec. VI.

*Electronic address: baer@mpipks-dresden.mpg.de

†Electronic address: aric@lanl.gov

URL: <http://math.lanl.gov/~aric>

‡Electronic address: ehud@bgumail.bgu.ac.il

§Electronic address: thiele@nolineal.pluri.ucm.es

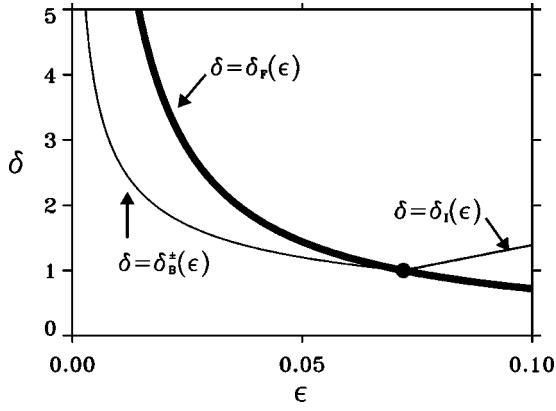


FIG. 1. The NIB bifurcation and planar-front transverse instability boundaries in the ϵ - δ parameter plane for a symmetric ($a_0 = 0$) and isotropic model. The thick curve is the NIB bifurcation, $\delta_F(\epsilon) = \eta_c^2/\epsilon$. The thin curves are the boundaries for the transverse instability of Ising, $\delta_I(\epsilon)$, and Bloch, $\delta_B(\epsilon)$, fronts. When $\delta > \delta_I$ ($\delta > \delta_B$) planar Ising (Bloch) fronts are unstable to transverse perturbations. Other parameters: $a_1 = 2.0$ and $d = 0$.

II. REACTION-DIFFUSION MODEL

Phenomenological models with parameters deduced from experimental data have been developed for several surface reactions including CO oxidation on platinum surfaces [41]. The rate equations involve adsorption, desorption, dissociation, and reaction terms. The spatial coupling is provided by surface diffusion of some adsorbed species, where anisotropy of diffusion, intrinsic or induced by adsorbate coverages, is taken into account. Many qualitative features of models of this kind are captured by FitzHugh-Nagumo (FHN) models describing bistable media [29,31,32]. The specific model we choose to study is

$$\begin{aligned} \frac{\partial u}{\partial t} &= \frac{1}{\epsilon}(u - u^3 - v) + \frac{1}{\delta} \left[\nabla^2 u + d \frac{\partial^2 u}{\partial y^2} \right], \\ \frac{\partial v}{\partial t} &= u - a_1 v - a_0 + \nabla^2 v, \end{aligned} \quad (1)$$

where u is the activator and v the inhibitor. The parameter a_1 is chosen so that Eqs. (1) represent a bistable medium with two stationary and uniform stable states, an ‘‘up’’ state, (u_+, v_+) , and a ‘‘down’’ state, (u_-, v_-) . Front solutions connect the two states. Figure 1 shows a diagram of front solutions in the parameter plane spanned by (ϵ, δ) for a symmetric ($a_0 = 0$) and isotropic ($d = 0$) system. For $\epsilon/\delta \ll 1$ the NIB bifurcation boundary is given by $\delta = \delta_F(\epsilon) = \eta_c^2/\epsilon$, or $\eta = \eta_c$, where $\eta = \sqrt{\epsilon\delta}$, $\eta_c = 3/2\sqrt{2}q^3$, and $q^2 = a_1 + 1/2$ [31]. The single stationary front (an ‘‘Ising’’ front) that exists for $\eta > \eta_c$ loses stability to a pair of counterpropagating fronts (‘‘Bloch’’ fronts) at $\eta = \eta_c$.

Also shown in Fig. 1 are boundaries for transverse instabilities, $\delta = \delta_I(\epsilon) = \epsilon/\eta_c^2$ and $\delta = \delta_B(\epsilon) = \eta_c/\sqrt{\epsilon}$, for Ising and Bloch fronts, respectively. Above these lines, $\delta > \delta_{I,B}$, planar fronts are unstable to transverse perturbations [35,34]. All three lines meet at the codimension 3 point: $\epsilon = \eta_c^2$, $\delta = 1$, $a_0 = 0$.

III. VELOCITY-CURVATURE RELATIONS

We study the effects of diffusion anisotropy by deriving velocity-curvature relations for nearly planar fronts. The derivation uses a singular perturbation approach and is valid for $\lambda := \sqrt{\epsilon/\delta} \ll 1$. Relations of this kind have proved invaluable for qualitative prediction of pattern formation processes in isotropic systems such as spot replication and spiral wave nucleation [34–36,42,43].

We transform to an orthogonal coordinate system (r, s) that moves with the front, where r is a coordinate normal to the front and s is the arclength. We denote the position vector of the front by $\mathbf{X}(s, t) = (X, Y)$, and define it to coincide with the $u = 0$ contour. The unit vectors tangent and normal to the front are given by

$$\hat{\mathbf{s}} = \cos \theta \hat{\mathbf{x}} + \sin \theta \hat{\mathbf{y}}, \quad \hat{\mathbf{r}} = -\sin \theta \hat{\mathbf{x}} + \cos \theta \hat{\mathbf{y}},$$

where $\theta(s, t)$ is the angle that $\hat{\mathbf{s}}$ makes with the x axis. A point $\mathbf{x} = (x, y)$ in the laboratory frame can be expressed as

$$\mathbf{x} = \mathbf{X}(s, t) + r \hat{\mathbf{r}}.$$

This gives the following relation between the laboratory coordinates (x, y, t) and the coordinates (s, r, τ) in the moving frame:

$$\begin{aligned} x &= X(s, t) - r \sin \theta(s, \tau), \\ y &= Y(s, t) + r \cos \theta(s, \tau), \\ t &= \tau. \end{aligned} \quad (2)$$

With this coordinate change, partial spatial derivatives transform according to

$$\begin{aligned} \frac{\partial}{\partial x} &= -\sin \theta \frac{\partial}{\partial r} + G \cos \theta \frac{\partial}{\partial s}, \\ \frac{\partial}{\partial y} &= \cos \theta \frac{\partial}{\partial r} + G \sin \theta \frac{\partial}{\partial s}, \end{aligned} \quad (3)$$

where

$$G = (1 + r\kappa)^{-1},$$

and κ , the front curvature, is given by

$$\kappa = -\frac{\partial \theta}{\partial s}.$$

The Laplacian becomes

$$\nabla^2 = \frac{\partial^2}{\partial r^2} + \kappa G \frac{\partial}{\partial r} + G \frac{\partial G}{\partial s} \frac{\partial}{\partial s} + G^2 \frac{\partial^2}{\partial s^2}. \quad (4)$$

The time derivative transforms according to

$$\frac{\partial}{\partial t} = \frac{\partial}{\partial \tau} - C_n \frac{\partial}{\partial r} + \dot{s} \frac{\partial}{\partial s}, \quad (5)$$

where

$$C_n = -\frac{\partial r}{\partial t} \quad (6)$$

is the front velocity in a direction normal to the front line. The time derivative of the arclength, \dot{s} , is generally nonzero due to stretching of the curved front line [40,44].

Using these derivative transformations in Eqs. (1) we obtain

$$\begin{aligned} 0 = & u - u^3 - v - \lambda \eta \left(\frac{\partial u}{\partial \tau} - C_n \frac{\partial u}{\partial r} + \dot{s} \frac{\partial u}{\partial s} \right) \\ & + \lambda^2 \left[(1 + d \cos^2 \theta) \frac{\partial^2 u}{\partial r^2} + \kappa G (1 + d \sin^2 \theta) \frac{\partial u}{\partial r} \right. \\ & \left. + dG \sin 2\theta \frac{\partial^2 u}{\partial r \partial s} + F(u; \partial_s) \right], \\ 0 = & u - a_1 v - a_0 - \left(\frac{\partial v}{\partial \tau} - C_n \frac{\partial v}{\partial r} + \dot{s} \frac{\partial v}{\partial s} \right) + \frac{\partial^2 v}{\partial r^2} \\ & + \kappa G \frac{\partial v}{\partial r} + G \frac{\partial G}{\partial s} \frac{\partial v}{\partial s} + G^2 \frac{\partial^2 v}{\partial s^2}, \end{aligned} \quad (7)$$

where $F(u; \partial_s)$ consists of terms involving partial derivatives of u with respect to s only.

Since $\lambda \ll 1$ we distinguish between an inner region where $\partial u / \partial r \sim \mathcal{O}(\lambda^{-1})$ and $\partial v / \partial r \sim \mathcal{O}(1)$, and outer regions where both $\partial u / \partial r$ and $\partial v / \partial r$ are of order unity. Consider first the inner region. Introducing a stretched normal coordinate $z = r/\lambda$ we obtain

$$\begin{aligned} 0 = & u - u^3 - v + (1 + d \cos^2 \theta) \frac{\partial^2 u}{\partial z^2} + \lambda \left[-\eta \frac{\partial u}{\partial \tau} \right. \\ & \left. + \eta V_n \frac{\partial u}{\partial z} - \eta \dot{s} \frac{\partial u}{\partial s} + \kappa G (1 + d \sin^2 \theta) \frac{\partial u}{\partial z} \right. \\ & \left. + dG \sin 2\theta \frac{\partial^2 u}{\partial z \partial s} \right] + \mathcal{O}(\lambda^2), \end{aligned} \quad (8)$$

where $V_n = C_n/\lambda$. Since $\partial v / \partial z = \lambda \partial v / \partial r \sim \mathcal{O}(\lambda)$ we can assume that $v = v_f$ is constant in the stretched coordinate system. We identify v_f with the value of v at $r=0$.

Expanding u and v_f as

$$\begin{aligned} u &= u_0 + \lambda u_1 + \lambda^2 u_2 + \dots, \\ v_f &= v_{f0} + \lambda v_{f1} + \lambda^2 v_{f2} + \dots, \end{aligned}$$

we find at order unity the stationary front solution

$$u_0 = -\tanh\left(\frac{z}{I(\theta)\sqrt{2}}\right), \quad v_{f0} = 0,$$

where

$$I(\theta) = \sqrt{1 + d \cos^2 \theta}.$$

At order λ we find the equation

$$\begin{aligned} \mathcal{L}u_1 = & v_{f1} - \eta V_n \frac{\partial u_0}{\partial z} + \eta \frac{\partial u_0}{\partial \tau} + \eta \dot{s} \frac{\partial u_0}{\partial s} \\ & - (1 + d \sin^2 \theta) \kappa G \frac{\partial u_0}{\partial z} - dG \sin 2\theta \frac{\partial^2 u_0}{\partial z \partial s}, \end{aligned} \quad (9)$$

where

$$\mathcal{L} = I(\theta)^2 \frac{\partial^2}{\partial z^2} + 1 - 3u_0^2. \quad (10)$$

The dependence of u_0 on s and τ comes through the dependence on θ . Thus,

$$\frac{\partial u_0}{\partial s} = -\frac{\kappa d \sin 2\theta}{2I^2} z \frac{\partial u_0}{\partial z},$$

and $\partial u_0 / \partial \tau \propto z \partial u_0 / \partial z$ as well. Projecting the right-hand side of Eq. (9) on the translational mode $\partial u_0 / \partial z$ (zero eigenmode of $\mathcal{L} = \mathcal{L}^\dagger$) we find

$$C_n = -\frac{3}{\eta\sqrt{2}} I(\theta) v_{f1} - \frac{1+d}{\delta I(\theta)^2} \kappa, \quad (11)$$

where we used the relations $v_f = \lambda v_{f1} + \mathcal{O}(\lambda^2)$ and $C_n = \lambda V_n$. We also approximated $G \approx 1$ assuming curvature is at most of order unity. Note that the terms $\eta \partial u_0 / \partial \tau$ and $\eta \dot{s} \partial u_0 / \partial s$ are orthogonal to the translational mode and therefore do not contribute to Eq. (11). Equation (11) shows how the normal front velocity is affected by the system's anisotropy.

We consider now the outer regions to the left and to the right of the inner, front region where $\partial u / \partial r \sim \partial v / \partial r \sim \mathcal{O}(1)$. The analysis of these regions (along the lines of Ref. [35]) will result in a second relation between C_n and v_f . Going back to the unstretched system (7), we find at leading order equations

$$0 = u - u^3 - v,$$

$$0 = u - a_1 v - a_0 + C_n \frac{\partial v}{\partial r} + \frac{\partial^2 v}{\partial r^2} + \kappa G \frac{\partial v}{\partial r}, \quad (12)$$

where we neglected time dependence in the moving frame and arclength dependence. This approximation is not valid when front transitions take place as they involve explicit time dependence of v in the moving frame. It is also not valid when spiral waves form because of the non-negligible variations along the arclength. For suitable a_1 values (typically about five or larger) the roots of Eq. (12) can be linearized around $v=0$. The extreme roots are then $u_\pm(v) = \pm 1 - v/2$. Using these forms in Eq. (12) we find the following boundary value problem for a front approaching the $(u_+, v_+)[(u_-, v_-)]$ state as $r \rightarrow -\infty (r \rightarrow +\infty)$:

$$\frac{\partial^2 v}{\partial r^2} + (C_n + \kappa G) \frac{\partial v}{\partial r} - q^2 v + q^2 v_+ = 0,$$

$$v(r=0) = v_f, \quad v(-\infty) = v_+, \quad r < 0, \quad (13)$$

$$\frac{\partial^2 v}{\partial r^2} + (C_n + \kappa G) \frac{\partial v}{\partial r} - q^2 v + q^2 v_- = 0,$$

$$v(r=0) = v_f, \quad v(+\infty) = v_-, \quad r > 0, \quad (14)$$

where

$$v_{\pm} = \frac{\pm 1 - a_0}{q^2}, \quad q^2 = a_1 + \frac{1}{2}. \quad (15)$$

For simplicity we would like to approximate $G \approx 1$ again. Since G multiplies now the derivative $\partial v / \partial r$ whose variation scale is of order unity we must require $|\kappa| \ll 1$. With this approximation Eqs. (13) and (14) admit the solutions

$$v(r) = (v_f - v_+) \exp \sigma_1 r + v_+, \quad r < 0,$$

$$v(r) = (v_f - v_-) \exp \sigma_2 r + v_-, \quad r > 0, \quad (16)$$

where

$$\sigma_{1,2} = -\frac{C_n + \kappa}{2} \pm \sqrt{\frac{(C_n + \kappa)^2}{4} + q^2}. \quad (17)$$

By construction, the outer solution (16) is continuous at $r = 0$. Demanding continuity of the derivative $\partial v / \partial r$ at $r = 0$ as well gives the second relation between C_n and v_f ,

$$v_f = -\frac{C_n + \kappa}{q^2 \sqrt{(C_n + \kappa)^2 + 4q^2}} - \frac{a_0}{q^2}. \quad (18)$$

Eliminating v_f by inserting Eq. (18) into Eq. (11) gives an implicit relation between the normal velocity of the front and its curvature

$$C_n + \frac{1+d}{\delta I(\theta)^2} \kappa = \frac{3I(\theta)(C_n + \kappa)}{\eta \sqrt{2} q^2 \sqrt{(C_n + \kappa)^2 + 4q^2}} + \frac{3I(\theta)a_0}{\eta \sqrt{2} q^2}. \quad (19)$$

Alternatively, we can eliminate C_n by inserting Eq. (11) into Eq. (18) to get an implicit relation between v_f and κ .

Typical velocity-curvature relations obtained as solutions of Eq. (19) for a given θ value are shown in Fig. 2. The number of intersection points with the $\kappa = 0$ axis indicates the number of planar front solutions. Positive slopes at these points indicate instabilities to transverse perturbations. Termination points of lower or upper branches close to the $\kappa = 0$ axis indicate proximity to the NIB bifurcation and a likelihood for spontaneous front transitions, that is, dynamic transitions between the two branches leading to reversals in the direction of front propagation [35–37,43]. These transitions can be induced by curvature variations, as Fig. 2 suggests, as well as by other perturbations like front interactions. Relations between the front velocity and its distance to a nearby front or a boundary can be similarly derived [45].

IV. STABILITY OF PLANAR FRONTS

Equation (19) can be used to study the effects of anisotropy on the stability properties of planar fronts. We begin with the NIB bifurcation. Consider the symmetric model with $a_0 = 0$. Setting $\kappa = 0$ we find the Ising front solution

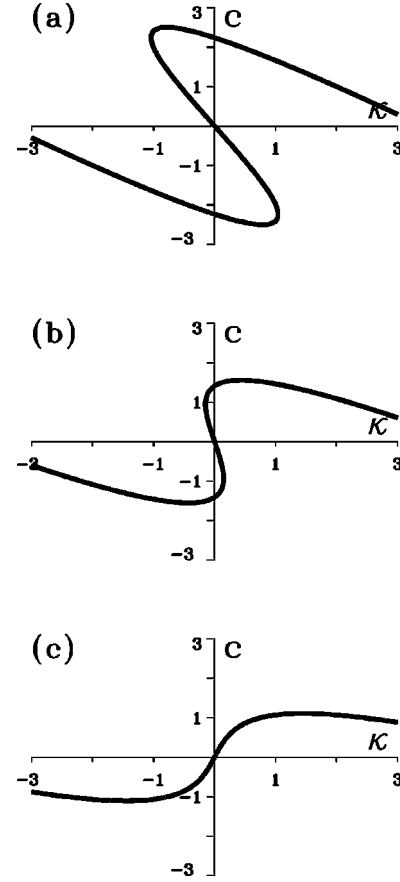


FIG. 2. Typical velocity-curvature relations of Eq. (19). (a) In the ‘‘Bloch regime’’ where both planar front solutions exist and are stable to transverse perturbations, $\delta = 1.2$. (b) Near the front bifurcation where two planar front solutions exist but are unstable to transverse perturbations. The solution branches terminate near small values of the curvature κ , $\delta = 1.5$. (c) In the ‘‘Ising regime’’ only a single (in this case transversely unstable) planar front exists, $\delta = 2.5$. Other parameters: $a_1 = 2.0$, $a_0 = 0.0$, $\epsilon = 0.04$.

$C_0 = 0$ and the two Bloch front solutions

$$C_0 = \pm \frac{2q}{\eta} \sqrt{\eta_c^2 I^2(\theta) - \eta^2}, \quad (20)$$

for $\eta < \eta_c I(\theta)$, where η_c is the NIB bifurcation point for the isotropic system and we recall that $\eta = \sqrt{\epsilon \delta}$. We have used here the notation C_0 for the velocity of a planar front. The anisotropy shifts the bifurcation point by the factor $1 \leq I \leq 1 + d$

$$\eta_c^{\text{anis}}(\theta) = \eta_c I(\theta). \quad (21)$$

In the ϵ - δ plane the front bifurcation line is given by

$$\delta = \delta_F = \frac{9}{8q^6} \frac{I^2(\theta)}{\epsilon}. \quad (22)$$

The stability of the Ising and Bloch fronts to transverse perturbations can be studied by linearizing Eq. (19) around $\kappa = 0$. This yields relations of the form

$$C_n = C_0 - D\kappa, \quad (23)$$

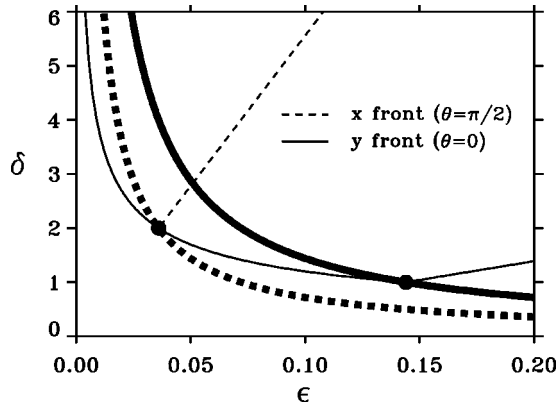


FIG. 3. The NIB bifurcation and planar-front transverse instability boundaries in the ϵ - δ parameter plane for the symmetric ($a_0 = 0$) and anisotropic ($d \neq 0$) case. The dashed lines are for the case of planar fronts propagating in the x direction ($\theta = \pi/2$) and the solid lines are for planar fronts propagating in the y direction ($\theta = 0$). The thick curves are the front bifurcation and the thin lines are the transverse instability boundaries of Ising and Bloch fronts. Note that the transverse instability boundaries for Bloch fronts in the x and y directions coincide. Parameters: $a_1 = 2$, $a_0 = 0$, $d = 1$.

where C_0 is one of the three front solutions (an Ising front and a pair of Bloch fronts). The condition $D=0$ gives the transverse instability threshold of the planar front solution in question. For the symmetric system ($a_0 = 0$) we obtain

$$\delta = \delta_I = \frac{8q^6 (1+d)^2 \epsilon}{9 I^6(\theta)}, \quad (24)$$

for the Ising front, and

$$\delta = \delta_B = \frac{3}{2\sqrt{2}q^3} \frac{\sqrt{1+d}}{\sqrt{\epsilon}}, \quad (25)$$

for the Bloch fronts. Notice that the transverse instability threshold for Bloch fronts (in the symmetric case) are independent of the angle θ . Figure 3 shows the NIB bifurcation line and the transverse instability lines for $\theta=0$ (solid curves) and for $\theta = \pi/2$ (dashed curves) assuming a symmetric system, $a_0 = 0$.

In the nonsymmetric case ($a_0 \neq 0$) it is still possible to get a relatively simple analytical expression for the threshold of the NIB bifurcation, $\eta_c^{\text{anis}}(\theta)$. This threshold occurs when the $\kappa=0$ line is tangent to the cubic $C_n - \kappa$ curve that solves Eq. (19). We first solve for the value of C_n at this point by deriving Eq. (19) with respect to C_n and setting $d\kappa/dC_n = \kappa = 0$. Using this value of C_n in Eq. (19) with $\kappa=0$ gives the threshold

$$\eta_c^{\text{anis}}(\theta) = \eta_c I(\theta) (1 - a_0^{2/3})^{3/2}. \quad (26)$$

Figure 4 shows a diagram of front solutions for the nonsymmetric case (the counterpart of Fig. 3 for $a_0 \neq 0$).

V. FRONT DYNAMICS AND ASYMPTOTIC PATTERNS

Anisotropy may introduce mechanisms for pattern formation that do not exist in isotropic system. We explore new mechanisms using C_n vs κ curves in orthogonal directions,

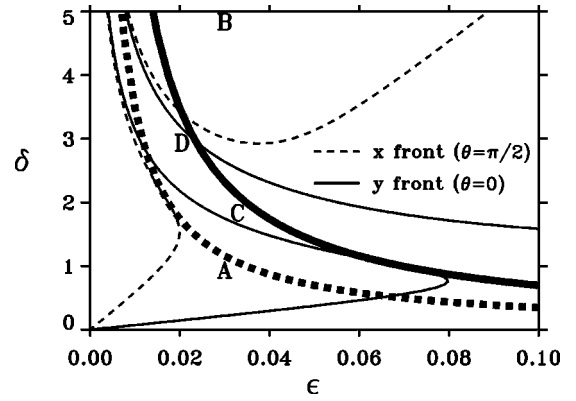


FIG. 4. The NIB bifurcation and planar-front transverse instability boundaries in the ϵ - δ parameter plane for the nonsymmetric ($a_0 \neq 0$) and anisotropic ($d \neq 0$) case. The dashed lines are for the case of planar fronts propagating in the x direction ($\theta = \pi/2$) and the solid lines are for planar fronts propagating in the y direction ($\theta = 0$). The thick curves are the front bifurcation and the thin lines are the transverse instability boundaries of Ising and Bloch fronts. Parameters: $a_1 = 2.0$, $a_0 = -0.1$, $d = 1.0$.

$\theta=0$ and $\theta = \pi/2$, paying attention to (i) the nature of planar-front solutions (Ising or counter-propagating Bloch fronts), (ii) the stability to transverse perturbations, (iii) the likelihood of front transitions (reversals).

The parameter space of interest here is the ϵ - δ plane at two values of the asymmetry parameter, a_0 , representing weak and strong asymmetries. The front bifurcation and the transverse instability boundaries in the ϵ - δ plane for the symmetric case ($a_0 = 0$) are shown in Fig. 3. Breaking the symmetry ($a_0 < 0$) removes the degeneracy of the two Bloch fronts (and their transverse instability boundaries) and leads to the diagram shown in Fig. 4. In the following, numerical solutions of Eq. (1) will be analyzed for parameters at each of the four points in this diagram, A, B, C, and D.

Shown in Fig. 5 are C_n vs κ curves for point A in the diagram. Both the x and y directions support pairs of counter-propagating Bloch fronts bounded away from the NIB bifurcation. The negative slopes of the Bloch front branches indicate stability to transverse perturbations in both directions. As a result stable traveling waves prevail [35]. Figure 6

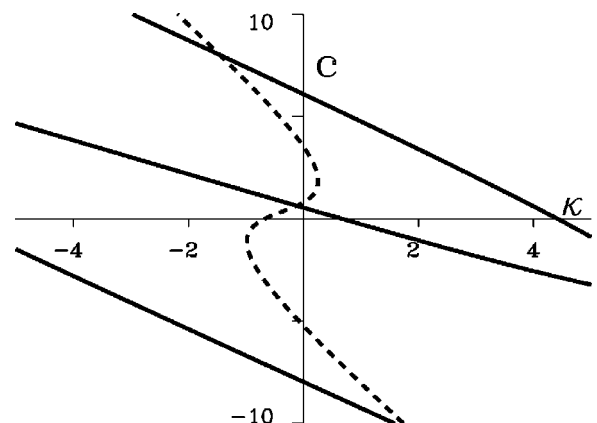


FIG. 5. Velocity vs curvature relation for the point A in Fig. 4. The solid (dashed) curves pertain to fronts propagating in the y (x) direction. Parameters: $a_1 = 2.0$, $a_0 = -0.1$, $\epsilon = 0.03$, $\delta = 0.8$.

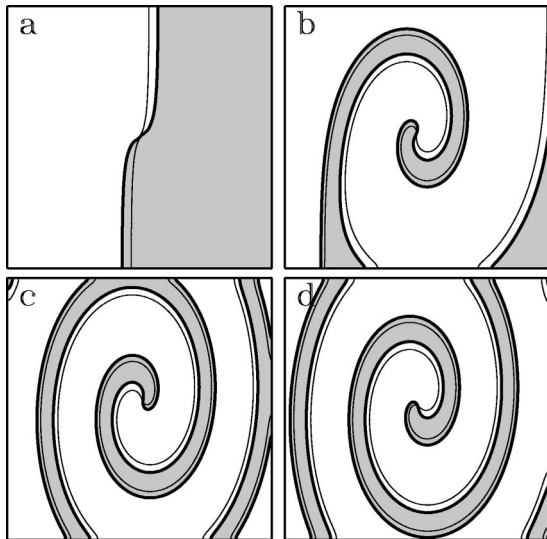


FIG. 6. Formation of an anisotropic spiral wave of Eq. (1) with the parameters chosen at point A in Fig. 4. Shaded regions are up-state domains. Thick (thin) lines are $u=0$ ($v=0$) contours. The $v=0$ line always lags behind the $u=0$ line.

shows an initial vortex structure evolving into a rotating spiral wave of elliptic shape due to the different propagation speeds at orthogonal directions.

At the other extreme, point B, both the x and y directions support Ising planar fronts, as implied by the C_n vs κ curves shown in Fig. 7. Fronts propagating in both directions are unstable to transverse perturbations, but in one direction, y , the instability is stronger. Choosing a stripe as an initial condition the strong transverse instability of fronts propagating in the y direction leads to fingering and eventually to a stationary periodic pattern oriented parallel to the y axis. The convergence toward a periodic stripe pattern is shown in Fig. 8. Changing the orientation of the initial stripe does not affect the nature of the asymptotic pattern; stripes are parallel to the y axis.

Notice that the weaker transverse instability of fronts propagating in the x direction is suppressed due to front interactions [46]. Similar behavior is expected when the difference in transverse instability strengths is greater or when a front propagating in the x direction is transversely stable. In

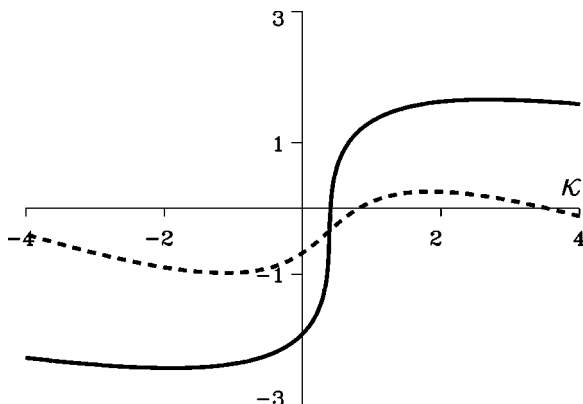


FIG. 7. Velocity vs curvature relation for the point B in Fig. 4. The solid (dashed) curves pertain to fronts propagating in the $y(x)$ direction. Parameters: $a_1=2.0$, $a_0=-0.1$, $\epsilon=0.03$, $\delta=5.0$.

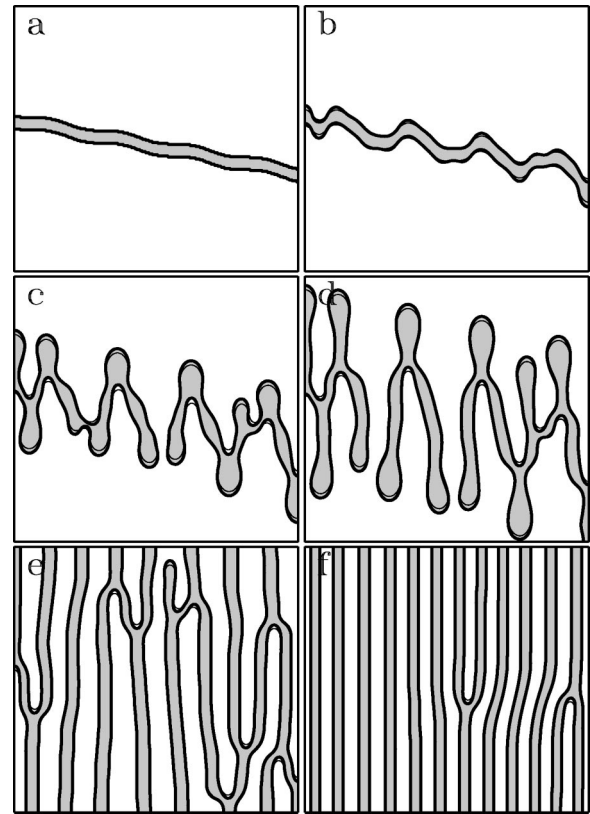


FIG. 8. Formation of a striped pattern with the parameters chosen at point B in Fig. 4. Fronts propagating in the x and y directions are both unstable to transverse perturbations but the instability is stronger in the y direction.

an isotropic system these initial conditions produce labyrinthine patterns provided the transverse instability of the Ising front is strong enough.

The pattern found at point C is more intricate. The corresponding C_n vs κ curves are shown in Fig. 9. The x direction supports a transversely stable Ising front whereas the y direction supports a pair of Bloch fronts. Starting with a disordered isotropic pattern the system evolves into a state we term stratified chaos. Strong irregular dynamics is confined to the y direction as indicated by the numerical solutions shown in Fig. 10. Segments oriented in that direction grow at

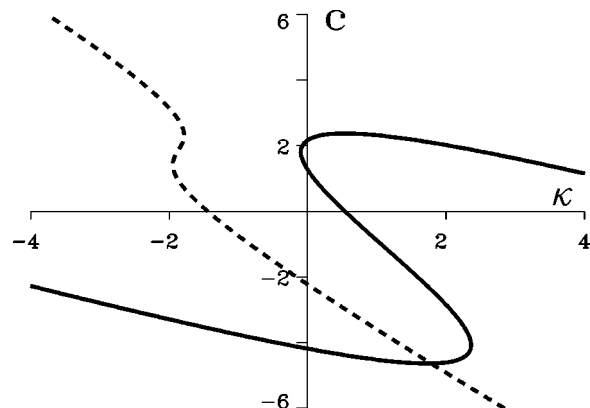


FIG. 9. Velocity-curvature relation for the point C in Fig. 4. The solid (dashed) curves pertain to fronts propagating in the $y(x)$ direction. Parameters: $a_1=2.0$, $a_0=-0.1$, $\epsilon=0.039$, $\delta=1.7$.

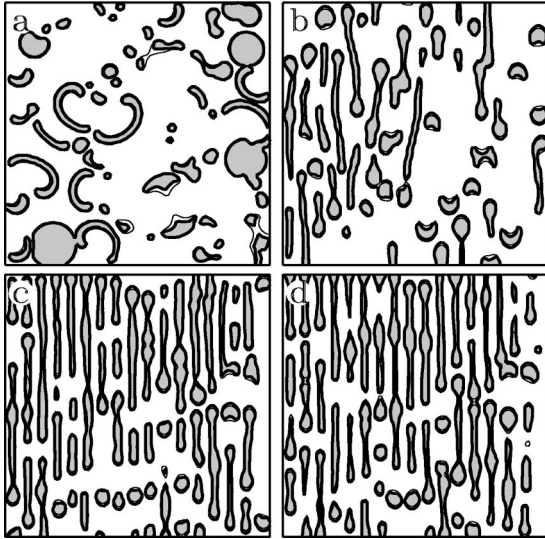


FIG. 10. Development of stratified chaos in Eq. (1) with parameters chosen at point C in Fig. 4.

their tips and either merge into larger segments or emit traveling blobs that grow new tips. In the x direction a nearly regular periodic structure is maintained. To quantify the irregular character of the dynamics in the y direction as compared with the regular character in the x direction we have computed the normalized spatial two-point correlation functions, $C_y(r)$ and $C_x(r)$, for the u field in both the x and y directions. These correlation functions are given by

$$C_y(r) = \frac{\langle \Delta u(x, y+r) \Delta u(x, y) \rangle}{\langle \Delta u(x, y)^2 \rangle},$$

$$C_x(r) = \frac{\langle \Delta u(x+r, y) \Delta u(x, y) \rangle}{\langle \Delta u(x, y)^2 \rangle},$$

where $\Delta u(x, y) = u(x, y) - \langle u \rangle$, and the brackets $\langle \rangle$ denote space and time averaging. Figure 11 shows the results of these computations. Correlations in the y direction decay to zero on a length scale much smaller than the system size, a feature characteristic to spatiotemporal chaotic systems. In contrast, correlations in the x direction oscillate with constant amplitude. This observation may be used to define stratified chaos as a state that displays finite correlation length in one direction (y) and infinite correlation length in the other (x).

A typical blob formation process occurring in the y direction is illustrated in Fig. 12. The mechanism for this process relies strongly on the transition from an Ising front in the x

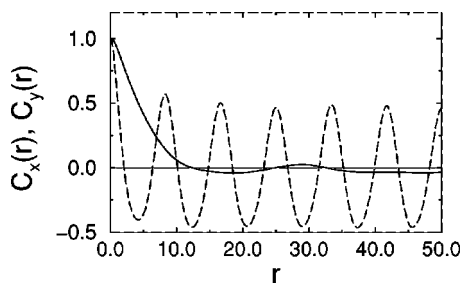


FIG. 11. Correlation functions $C_x(r)$ (dashed curve) and $C_y(r)$ (solid curve).

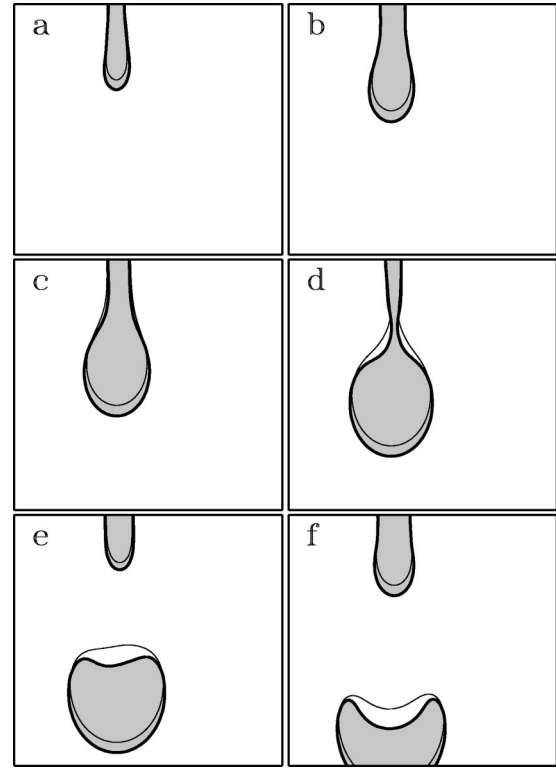


FIG. 12. Close up of repeated blob formation. Shaded regions are up-state domains. Thick (thin) curves are $u=0$ ($v=0$) contours. The $v=0$ contour always lags behind the $u=0$ contour. The tip of a stripe segment (a) grows outward (b)–(c). A pinching dynamic begins (d), which leads to blob formation (e) traveling along the y direction (f). The blob formation leaves a shortened stripe segment (e) whose tip grows outward again (f) and the process repeats. The parameters are the same as in Fig. 10.

direction to a Bloch front in the y direction. In the x direction a pair of fronts approaching one another (“white” invading “grey” fronts in Fig. 12) repel and form stationary or breathing stripes. In the y direction a pair of approaching fronts collapse and the domains following them merge. Imagine a segment tip growing into a bulge as in Figs. 12(a), 12(b), 12(c). At the neck of the bulge, propagation directions deviating from the x axis develop and front collapse may occur. This leads to the detachment of a traveling blob as shown in Figs. 12(d), 12(e). The reader is referred to Ref. [47] for further details about stratified chaos.

We conclude this section with the introduction of a fourth dynamical behavior (point D in Fig. 4). The C_n vs κ relation pertaining to this case is shown in Fig. 13. In the x direction, the system has an Ising front, which is stable to transverse perturbations and is close to the NIB bifurcation. In the y direction the system has Bloch fronts one or both of which are unstable to transverse perturbations. The transverse instability in the y direction leads to finger growth and stripe formation parallel to the y axis similar to the behavior found at point B in Fig. 8, but the proximity to the NIB bifurcation in the x direction allows for breathing stripes (see Fig. 14). The breathing motion involves repeated transitions between the counterpropagating Bloch fronts that are near the NIB bifurcation. The breathing amplitude is constant in time as shown in Fig. 15.

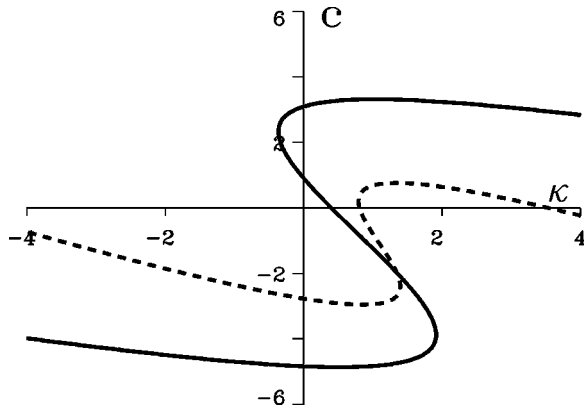


FIG. 13. Velocity-curvature relation for the point D , Fig. 4. The solid (dashed) curves pertain to fronts propagating in the $y(x)$ direction. Parameters: $a_1=2.0$, $a_0=-0.1$, $\epsilon=0.018$, $\delta=3.0$.

VI. CONCLUSION

We have explored a few examples of C_n vs κ relations and used them to identify parameter values where anisotropy plays a dominant role in pattern dynamics. One remarkable outcome is the ordering effect anisotropy has leading to periodic stationary stripe or periodic breathing stripe patterns (points B and D in Fig. 4). Another result is the transition of regular stripes to stratified chaos in parameter ranges where the angular dependence of front dynamics involves a change from an Ising front to Bloch fronts. An example where anisotropy has a trivial effect on pattern dynamics has also been demonstrated: the elliptically shaped spiral wave in the regime of transversely stable Bloch fronts.

We did not carry out a systematic study exploring all possible realizations of C_n vs κ curves in orthogonal directions: Ising fronts vs Bloch fronts, stability vs instability to transverse perturbations, different connectivities of the three-front solution branches in the Bloch regime at high curvature values, etc. A study of that kind may reveal many more

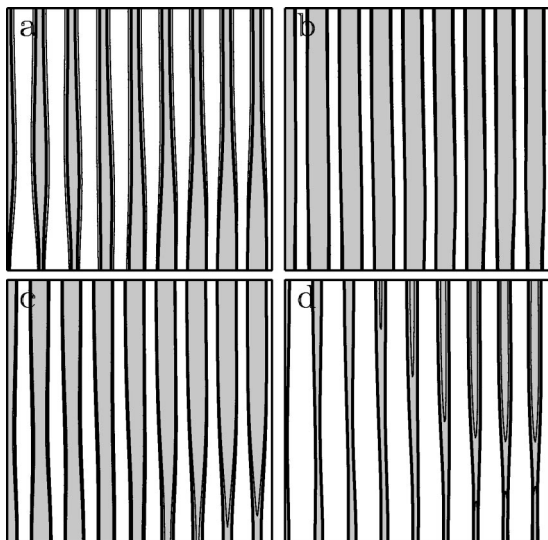


FIG. 14. Breathing stripes with parameters chosen at point D in Fig. 4 starting with the same initial conditions as in Fig. 8. After the initial transient formation of the stripes, the width of the stripes oscillates in time. The frames are at $t=74,76,78,80$.

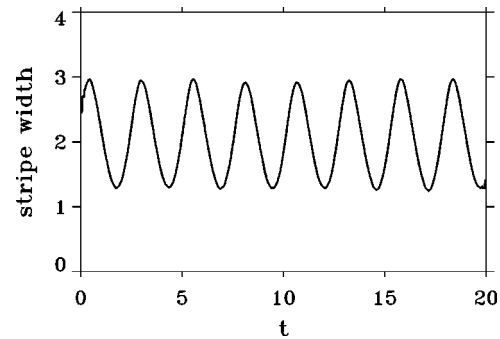


FIG. 15. Stripe width vs time for the breathing stripe solution. The curve represents oscillations in the width of a single stripe in the simulation of Fig. 14.

phenomena that can be attributed to the effect of anisotropic diffusion. These include in particular observed phenomena such as rectangular and triangular front shapes with sharp corners and traveling wave fragments [10,12,13,48–50]. We also did not study in detail the effects of front interactions or interactions with boundaries on pattern dynamics (e.g., front reversal or vortex nucleation). Relations between the velocities of interacting fronts, C , and the distances between them, d , can be derived using an approach similar to that used in deriving C_n vs κ relations [45].

A relation between the normal velocity of a front and its curvature can be used to evolve front lines in time [39] to simulate patterns such as spiral waves. This approach cannot be applied to the velocity-curvature relations derived in Sec. III because of the multivalued nature of these relations near the NIB bifurcation. The appropriate approach consists of coupled evolution equations for the curvature and the normal front velocity, which capture dynamic transitions between counterpropagating Bloch fronts. Such an approach has been developed for isotropic media in Refs. [37,43] but has not yet been extended to anisotropic systems.

The anisotropy considered here pertains to diffusion rates. Similar effects on pattern formation might be expected in systems with anisotropic advection caused by flows or electric fields [8] or in spatially heterogeneous systems with broken rotational symmetry. Examples for the latter are formation of waves with sharp corners in the Belousov-Zhabotinsky reaction with heterogeneous distribution of catalyst [51,52], elongated spirals and targets in heterogeneous media [53], or the production of ordered stripes in thin films of polymer mixtures on a striped substrate when a homogeneous substrate leads to labyrinthine patterns and coarsening [54].

ACKNOWLEDGMENTS

Part of the work of U.T. was supported by Grant No. D/98/14745 of the German Academic Exchange Board (DAAD). M. B. gratefully acknowledges the hospitality of Ben-Gurion University and support of the Max-Planck-Society (MPG). Part of this research is supported by the U.S. Department of Energy under Contract No. W-7405-ENG-36.

- [1] L. Kramer and W. Pesch, *Annu. Rev. Fluid Mech.* **27**, 515 (1995).
- [2] R. Imbihl and G. Ertl, *Chem. Rev.* **95**, 697 (1995).
- [3] A. T. Winfree, *Int. J. Bifurcation Chaos Appl. Sci. Eng.* **7**, 487 (1997).
- [4] J. Keener and J. Sneyd, *Mathematical Physiology* (Springer, New York, 1998).
- [5] A. T. Winfree, *Chaos* **8**, 1 (1998).
- [6] M. C. Cross and P. C. Hohenberg, *Rev. Mod. Phys.* **65**, 851 (1993).
- [7] M. Scheuring, L. Kramer, and W. Pesch, *Phys. Rev. E* **58**, 2018 (1998).
- [8] G. D. Granzow and H. Riecke, *Physica A* **249**, 27 (1998).
- [9] R. Faller and L. Kramer, *Phys. Rev. E* **57**, R2649 (1998).
- [10] F. Mertens and R. Imbihl, *Nature (London)* **370**, 124 (1994).
- [11] A. S. Mikhailov, *Phys. Rev. E* **49**, 5875 (1994).
- [12] N. Gottschalk, F. Mertens, M. Bär, M. Eiswirth, and R. Imbihl, *Phys. Rev. Lett.* **73**, 3483 (1994).
- [13] F. Mertens, N. Gottschalk, M. Bär, M. Eiswirth, A. Mikhailov, and R. Imbihl, *Phys. Rev. E* **51**, 5193 (1995).
- [14] M. Flytzani-Stephanopoulos and L. D. Schmidt, *Prog. Surf. Sci.* **9**, 83 (1979).
- [15] R. Imbihl, *Prog. Surf. Sci.* **33**, 183 (1993).
- [16] *Chemical Waves and Patterns*, edited by R. Kapral and K. Showalter (Kluwer Academic, Dordrecht, 1994).
- [17] H. H. Rotermund, *Surf. Sci. Rep.* **29**, 265 (1997).
- [18] M. Bär, C. Zülicke, M. Eiswirth, and G. Ertl, *J. Chem. Phys.* **96**, 8595 (1992).
- [19] M. Berdau, G. G. Yelenin, A. Karpowicz, M. Ehsasi, K. Christmann, and J. H. Block, *J. Chem. Phys.* **110**, 11551 (1999).
- [20] S. Nettesheim, A. von Oertzen, H. H. Rotermund, and G. Ertl, *J. Chem. Phys.* **98**, 9977 (1992).
- [21] M. Bär, N. Gottschalk, M. Eiswirth, and G. Ertl, *J. Chem. Phys.* **100**, 1202 (1994).
- [22] J. Lauterbach and H. H. Rotermund, *Surf. Sci.* **311**, 231 (1994).
- [23] M. Berdau, A. Karpowicz, G. G. Yelenin, K. Christmann, and J. H. Block, *J. Chem. Phys.* **106**, 4921 (1997).
- [24] M. Bär, S. Nettesheim, H. H. Rotermund, M. Eiswirth, and G. Ertl, *Phys. Rev. Lett.* **74**, 1246 (1995).
- [25] G. Haas, M. Bär, I. G. Kevrekidis, P. B. Rasmussen, H.-H. Rotermund, and G. Ertl, *Phys. Rev. Lett.* **75**, 3560 (1995).
- [26] K. J. Lee and H. L. Swinney, *Phys. Rev. E* **51**, 1899 (1995).
- [27] G. Li, Q. Ouyang, and H. L. Swinney, *J. Chem. Phys.* **105**, 10 830 (1996).
- [28] T. Frisch, Ph.D. thesis, Université de Nice Sophia-Antipolis, 1994.
- [29] H. Ikeda, M. Mimura, and Y. Nishiura, *Nonlin. Anal. TMA* **13**, 507 (1989).
- [30] P. Couillet, J. Lega, B. Houchmanzadeh, and J. Lajzerowicz, *Phys. Rev. Lett.* **65**, 1352 (1990).
- [31] A. Hagberg and E. Meron, *Nonlinearity* **7**, 805 (1994).
- [32] M. Bode, A. Reuter, R. Schmeling, and H.-G. Purwins, *Phys. Lett. A* **185**, 70 (1994).
- [33] C. Elphick, A. Hagberg, E. Meron, and B. Malomed, *Phys. Lett. A* **230**, 33 (1997).
- [34] A. Hagberg and E. Meron, *Phys. Rev. Lett.* **72** (15), 2494 (1994).
- [35] A. Hagberg and E. Meron, *Chaos* **4**, 477 (1994).
- [36] C. Elphick, A. Hagberg, and E. Meron, *Phys. Rev. E* **51**, 3052 (1995).
- [37] A. Hagberg and E. Meron, *Phys. Rev. Lett.* **78**, 1166 (1997).
- [38] R. C. Brower, D. A. Kessler, J. Koplik, and H. Levine, *Phys. Rev. A* **29**, 1335 (1984).
- [39] E. Meron and P. Pelcé, *Phys. Rev. Lett.* **60**, 1880 (1988).
- [40] A. S. Mikhailov, *Foundation of Synergetics I: Distributed Active Systems* (Springer-Verlag, Berlin, 1990).
- [41] G. Flätgen and K. Krischer, *J. Chem. Phys.* **103**, 5428 (1995).
- [42] A. Hagberg, E. Meron, I. Rubinstein, and B. Zaltzman, *Phys. Rev. E* **55**, 4450 (1997).
- [43] A. Hagberg and E. Meron, *Physica D* **123**, 460 (1998).
- [44] E. Meron, *Phys. Rep.* **218**, 1 (1992).
- [45] D. Haim, G. Li, Q. Ouyang, W. D. McCormick, H. L. Swinney, A. Hagberg, and E. Meron, *Phys. Rev. Lett.* **77**, 190 (1996).
- [46] A. Hagberg, E. Meron, and T. Passot, *Phys. Rev. E* **61**, 6471 (2000).
- [47] M. Bär, A. Hagberg, E. Meron, and U. Thiele, *Phys. Rev. Lett.* **83**, 2664 (1999).
- [48] A. Schaak and R. Imbihl, *Chem. Phys. Lett.* **283**, 386 (1998).
- [49] F. Mertens and R. Imbihl, *Surf. Sci.* **347**, 355 (1996).
- [50] A. Schaak and R. Imbihl, *J. Chem. Phys.* **107**, 4741 (1997).
- [51] S. P. Dawson, A. Lawniczak, and R. Kapral, *J. Chem. Phys.* **100**, 5211 (1994).
- [52] O. Steinbock, P. Kettunen, and S. C. Müller, *Science* **269**, 1857 (1995).
- [53] M. Bär, A. K. Bangia, Y. Kevrekidis, G. Haas, H.-H. Rotermund, and G. Ertl, *J. Chem. Phys.* **100**, 19106 (1996).
- [54] M. Böltau, S. Walheim, J. Mlynek, G. Krausch, and U. Steiner, *Nature (London)* **391**, 871 (1998).